Journal of Engineering Mechanics and Machinery (2025)
Clausius Scientific Press, Canada

DOI: 10.23977/jemm.2025.100102
ISSN 2371-9133 Vol. 10 Num. 1

Numerical Simulation Study of NACA2415 Airfoil Using PANS Model Based on User-Defined Functions

Yu Yunyun[1,a,*], Yang Tianhe[1], Zhou Daqing[2]

[1]School of Air Transportation and Engineering, Nanhang Jincheng College, Nanjing, China
[2]College of Energy & Electrical Engineering, Hohai University, Nanjing, China
[a]yuyunyun@nhjcxy.edu.cn
[*]Corresponding author

Keywords: UDF, PANS, NACA2415, Numerical Simulation

Abstract: This paper constructs a Partially-Averaged Navier-Stokes (PANS) turbulence model using User-Defined Function (UDF) programming based on FLUENT software and applies it to the numerical simulation study of the NACA2415 airfoil. Through the secondary development of FLUENT, the construction and validation of the PANS model were successfully achieved. The flow field characteristics of the NACA2415 airfoil at different angles of attack were calculated, and the lift coefficient was monitored and compared with wind tunnel experimental results. The study showed that the PANS model effectively captures the velocity streamlines and pressure variations on the surface of the airfoil, demonstrating a high predictive accuracy compared to experimental data. This research provides a technical reference for the simulation of complex flow fields and the optimization of turbulence modeling methods.

1. Introduction

With the rapid advancement of aerospace technology, the requirements for accuracy and efficiency in aircraft design are continuously increasing. In this process, aerodynamic design has become one of the key factors determining aircraft performance. As the primary aerodynamic component of an aircraft, the airfoil design directly affects flight performance, including critical parameters such as lift, drag, and stability. Traditional airfoil design methods rely on wind tunnel experiments and empirical formulas. However, these approaches have limitations in complex flow field environments, particularly under conditions of high Mach numbers and supercritical flows, where they fail to fully capture the aerodynamic characteristics of real flight conditions.

Computational Fluid Dynamics (CFD), as a powerful numerical simulation tool, has been widely applied in the aerospace field. By employing CFD methods, it is possible to accurately simulate the aerodynamic performance of an aircraft's airfoil under various flight conditions, including flow field distribution, pressure variations, and aerodynamic coefficients, providing a theoretical foundation for airfoil optimization. CFD simulations not only reduce experimental costs and development cycles but also offer more comprehensive and detailed flow information. This is particularly valuable in the early design stages, where different airfoil configurations can be rapidly evaluated for performance.

When using CFD to simulate airfoils, the most critical factor is the accurate modeling of turbulence.

Although traditional turbulence models, such as the k-ε and k-ω models, have been widely applied in engineering practice, their accuracy and adaptability remain limited under complex flow conditions involving strong shear, separation, or recirculation. Consequently, improving existing turbulence models to enhance their predictive accuracy in complex flow environments has become a key research focus.

Among these efforts, hybrid-precision turbulence models, such as the Partially-Averaged Navier-Stokes (PANS) model, have emerged as an important research direction [1]. The PANS model integrates the advantages of Large Eddy Simulation (LES) and Reynolds-Averaged Navier-Stokes (RANS) models, enabling it to provide more refined turbulence information in critical flow regions without significantly increasing computational costs.

In recent years, significant progress has been made in the research of the PANS turbulence model both domestically and internationally. Girimaji et al. first proposed the PANS model, introducing adjustable resolution parameters to organically combine the averaging characteristics of the RANS model with the high-resolution features of the LES model, providing an efficient alternative for the numerical simulation of complex turbulence [2].

Chinese researchers have also achieved important advancements in turbulence modeling and its engineering applications. Many research institutions and universities, such as Tsinghua University and Xi'an Jiaotong University, have conducted in-depth studies on the implementation and optimization of the PANS model [3-4]. By incorporating User-Defined Functions (UDFs), domestic researchers have successfully applied the PANS model to the prediction of flow characteristics in turbine blades, vehicle aerodynamics, and complex structures, yielding results that are largely consistent with experimental data [5].

Currently, research on the PANS model for airfoil flow characteristics in atmospheric conditions remains limited. In particular, further validation is needed regarding its applicability and reliability in aerodynamic performance prediction and capturing complex flow separation behaviors. As a representative aircraft airfoil, the NACA2415 airfoil is an ideal subject for turbulence model studies due to its extensive engineering applications and abundant wind tunnel test data. In this study, the PANS model is implemented through User-Defined Function (UDF) programming via secondary development in Fluent to conduct numerical simulations of the NACA2415 airfoil. The objective is to comprehensively evaluate the accuracy of the PANS model in simulating the aerodynamic performance of airfoils.

2. Airfoil Model

The airfoil used in this study is NACA 2415, a classic design from the four-digit series airfoils developed by the National Advisory Committee for Aeronautics (NACA). It has been widely applied in the aerospace field and is supported by extensive theoretical research and wind tunnel experimental data [6]. The aerodynamic characteristics of NACA 2415, including lift coefficient, drag coefficient, and stall behavior, have been tested in wind tunnels and recorded in NASA's publicly available database, providing a reliable benchmark for validating CFD numerical simulation results.

The NACA 2415 airfoil was modeled with a chord length of 1 meter to analyze its flow characteristics. During the computation, the lift coefficient was monitored and compared with wind tunnel experimental data. Figure 1 illustrates the computational domain of the NACA 2415 airfoil. The ICEM CFD 16.0 software was used to generate a hexahedral structured mesh, with an initial total mesh count of approximately 30,000 and a mesh quality above 0.85. Figure 2 presents the mesh quality of the computational domain.

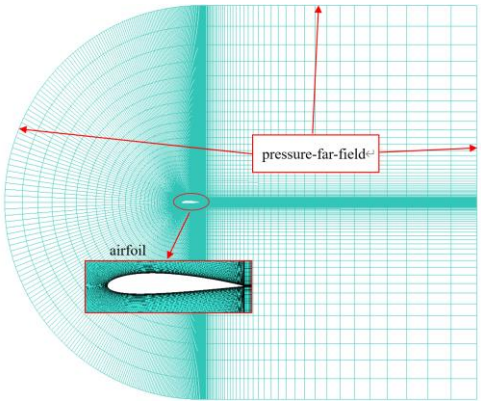

Figure 1: Computational Domain and Mesh Generation of the NACA 2415 Airfoil

Figure 2: Mesh Quality of the Computational Domain

After the initial trial computation, the '$Y+$' value was examined in Fluent. Using Fluent's mesh adaptation, the wall mesh was refined to maintain the '$Y+$' value within the range of 30 to 100. Figure 3 shows the result of the adaptive mesh refinement on the airfoil surface.

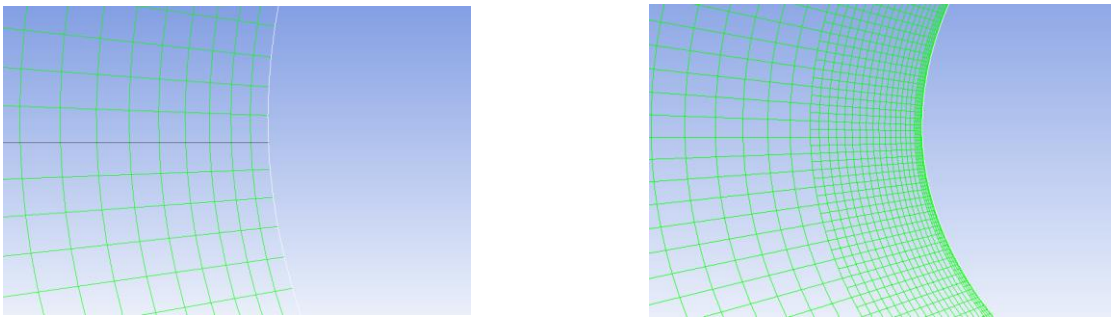

(a) Before Mesh Adaptation (b) After Mesh Adaptation

Figure 3: Mesh Adaptation of the Airfoil Surface

3. Solution Method

3.1 Turbulence Model

Numerical calculations were performed using Fluent, with modifications to the turbulence model implemented via the User-Defined Function (UDF) feature. The motion of fluid dynamics follows the principles of mass conservation, momentum conservation, and energy conservation, which together form the fundamental equations of fluid mechanics [7].

(1) Continuity Equation (Mass Conservation Law)

$$\frac{\partial \rho}{\partial t} + \nabla \cdot (\rho \mathbf{u}) = 0 \tag{1}$$

In the equation, ρ represents density, $\mathbf{u}$ is the velocity vector, where $\mathbf{u}=(u,v,w)$, and t denotes time.

(2) Momentum Conservation Equation (Navier-Stokes Equation):

$$\frac{\partial (\rho u)}{\partial t} + \nabla \cdot (\rho u \mathbf{u}) = -\frac{\partial p}{\partial x} + \nabla \cdot \tau_x \tag{2}$$

$$\frac{\partial(\rho v)}{\partial t} + \nabla\cdot(\rho v\mathbf{u}) = -\frac{\partial p}{\partial y} + \nabla\cdot\tau_y$$

$$\frac{\partial(\rho w)}{\partial t} + \nabla\cdot(\rho w\mathbf{u}) = -\frac{\partial p}{\partial z} + \nabla\cdot\tau_z$$

In the equation, τ_x, τ_y and τ_z represent the components of the viscous stress tensor, where $\tau_x=\mu(\frac{\partial u}{\partial x} - \frac{1}{3}\nabla\cdot\mathbf{u})$, with similar expressions for the y and z directions.

(3) Energy Conservation Equation:

$$\frac{\partial(\rho e_t)}{\partial t} + \nabla\cdot(\rho e_t\mathbf{u}) = -\nabla\cdot(p\mathbf{u}) + \nabla\cdot(k\nabla\mathrm{T}) + \Phi \tag{3}$$

In the equation, e_t represents the total energy density, which includes internal energy (e) and kinetic energy. $e_t=e+\frac{1}{2}|\mathbf{u}|^2$. T represents temperature, k is the thermal conductivity, and Φ denotes the viscous dissipation term, which accounts for energy loss due to viscosity. $\Phi=\mu\left[(\frac{\partial u}{\partial x})^2+(\frac{\partial v}{\partial y})^2+(\frac{\partial w}{\partial z})^2\right]$.

CFD numerical calculations utilize the rapid iterative capabilities of computers to discretize and solve the governing equations progressively. In the process of solving the Navier-Stokes (N-S) equations, numerical methods are classified, in order of decreasing accuracy, into three approaches: Direct Numerical Simulation (DNS), Large Eddy Simulation (LES), and Reynolds-Averaged Navier-Stokes (RANS) simulation [8].

DNS directly solves the Navier-Stokes equations, capturing all flow details without turbulence modeling. However, it requires extremely fine meshes and very small time step size, leading to high computational and economic costs. Due to these demands, DNS is typically used for simple low-Reynolds-number flows. LES applies a filtering technique to separate turbulence into large-scale and small-scale structures. The small-scale fluctuations are modeled, while the large-scale structures are directly resolved from the governing equations. For high-Reynolds-number flows (e.g., aerodynamic simulations of aircraft), LES still requires sufficiently fine meshes and small time step size to capture large eddy dynamics, making its computational cost potentially close to DNS. RANS (Reynolds-Averaged Navier-Stokes Simulation): Unlike DNS and LES, RANS does not resolve turbulence scales directly. Instead, it averages the flow field using Reynolds decomposition, breaking it into a mean flow component and a fluctuating component. The turbulent fluctuations are approximated using turbulence models, significantly reducing computational costs. However, RANS relies heavily on turbulence models, and its ability to capture complex flow details is limited, particularly in flows involving separation, recirculation, or strong shear layers.

The RANS turbulence models include: zero-equation models (e.g., Prandtl model), one-equation models (e.g., Spalart-Allmaras model), and two-equation models (e.g., k-ε model and k-ω model). The turbulence model used in this study is the Partially-Averaged Navier-Stokes (PANS) model, which is a customized version based on the k-ε model. The PANS model adjusts the resolution of the turbulence model to control the level of equation resolution, enabling a transition from fully turbulence-averaged (RANS) to transient turbulence resolution (approaching LES). This approach is well-suited for the study of turbulent characteristics in complex flows, while maintaining a balance between computational cost and accuracy.

Applying time-averaging to the Navier-Stokes equations using the RANS method:

$$\frac{\partial\bar{\mathbf{u}}}{\partial t} + \bar{\mathbf{u}}\cdot\nabla\bar{\mathbf{u}} = -\frac{1}{\rho}\nabla\bar{p} + \nu\nabla^2\bar{\mathbf{u}} - \nabla\cdot\overline{\mathbf{u}'\otimes\mathbf{u}'} \tag{4}$$

$\frac{\partial \bar{\mathbf{u}}}{\partial t}$ represents the unsteady term of the mean velocity, $\bar{\mathbf{u}} \cdot \nabla \bar{\mathbf{u}}$ is the convective term, describing the momentum transport of the mean flow, $-\frac{1}{\rho}\nabla \bar{p}$ is the mean pressure gradient term, $\nu \nabla^2 \bar{\mathbf{u}}$ is the viscous diffusion term, which accounts for the dissipation effect of viscosity on momentum, $\nabla \cdot \overline{\mathbf{u}' \otimes \mathbf{u}'}$ is the Reynolds stress term, describing the additional effect of turbulent fluctuations on the mean flow.In the RANS method, the *k*-*ε* model achieves closure of the Reynolds stress term by solving the turbulent kinetic energy (*k*) and the turbulence dissipation rate (*ε*).

The PANS model, based on the *k*-*ε* model, partially decomposes the Reynolds stress to obtain the Navier-Stokes equations [9]:

$$\frac{\partial \tilde{\mathbf{u}}}{\partial t} + \tilde{\mathbf{u}} \cdot \nabla \tilde{\mathbf{u}} = -\frac{1}{\rho}\nabla \tilde{p} + \nu \nabla^2 \tilde{\mathbf{u}} - \nabla \cdot \tau_{ij} \tag{5}$$

$\tilde{\mathbf{u}}$ represents the partially-averaged velocity, τ_{ij} is the sub grid-scale stress tensor, given by $\tau_{ij} = \overline{u_i' u_j'} f_k$. The parameters f_k and f_ε are introduced to define the ratio of resolved and unresolved turbulence components, adjusting the turbulence transport equations, which mainly include:

Turbulent Kinetic Energy (*k*) Equation:

$$\frac{\partial(\rho k)}{\partial t} + \nabla \cdot (\rho \mathbf{u} k) = \nabla \cdot \left[(\mu + \frac{\mu_t}{\sigma_k}) \nabla k \right] + P_k - \rho \varepsilon \tag{6}$$

In the equation, μ represents the molecular dynamic viscosity, μ_t is the turbulent viscosity, σ_k is the Prandtl number for turbulent kinetic energy diffusion, and P_k denotes the turbulence production term. $P_k = \tau_{ij} \frac{\partial u_i}{\partial x_j}$

Turbulence Dissipation Rate (*ε*) Equation:

$$\frac{\partial(\rho \varepsilon)}{\partial t} + \nabla \cdot (\rho \mathbf{u} \varepsilon) = \nabla \cdot \left[(\mu + \frac{\mu_t}{\sigma_\varepsilon}) \nabla \varepsilon \right] + C_{1\varepsilon} \frac{\varepsilon}{k} P_k - C_{2\varepsilon} \rho \frac{\varepsilon^2}{k} \tag{7}$$

In the equation, σ_ε is the Prandtl number for turbulence dissipation diffusion, $C_{1\varepsilon} \frac{\varepsilon}{k} P_k$ represents the turbulence production term, and $C_{2\varepsilon} \rho \frac{\varepsilon^2}{k}$ denotes the turbulence dissipation term. $C_{1\varepsilon}$ and $C_{2\varepsilon}$ are model constants, typically determined empirically. These two equations are coupled through the production and dissipation terms, influencing the calculation of the turbulent viscosity (μ_t), given by: $\mu_t = \rho C_\mu \frac{k^2}{\varepsilon}$, where C_μ is an empirical coefficient, generally set to 0.09 [10].

Turbulent Kinetic Energy Resolution Parameter:

$$f_k = \frac{k}{k_t} \tag{8}$$

In the equation, *k* represents the resolved turbulent kinetic energy, k_t is the total turbulent kinetic energy, f_k denotes the ratio of resolved turbulent kinetic energy, where $0 < f_k \leqslant 1$.

Turbulence Dissipation Rate Resolution Parameter:

$$f_\varepsilon = \frac{\varepsilon}{\varepsilon_t} \tag{9}$$

In the equation, *ε* is the turbulent dissipation rate being currently analyzed, ε_t is the total turbulent dissipation rate, and f_ε represents the proportion of the analyzed turbulent dissipation rate, where $0 < f_\varepsilon \leqslant 1$.

f_k is an explicit parameter that directly affects the sub grid stress tensor τ_{ij} in the momentum equation. f_ε is an implicit parameter that indirectly influences the simulation results by affecting the turbulent energy dissipation process.

According to extensive literature studies, $f_\varepsilon = 1$ is more appropriate for high Reynolds number flows. However, the choice of f_k has a significant impact on the computational results [11]. When $f_k = 1$, the PANS model completely degenerates into the RANS model. When $f_k = 0$, the resolved turbulence ratio increases, making PANS approach the LES model. As f_k increases from a lower value, the PANS model smoothly transitions from LES to RANS.A smaller f_k value allows for higher resolution results, but it also substantially increases the mesh size and computational cost. Therefore, in PANS simulations, the selection of f_k is particularly critical.

In this study, the UDF (User-Defined Function) feature in Fluent was utilized, and C language was programmed in Visual Studio to define custom expressions for f_k and f_ε. The 'DEFINE_SOURCE' macro was employed to modify the source terms of turbulent kinetic energy and dissipation rate. The UDF was then compiled, loaded into Fluent, and incorporated into the turbulence equations, with the $k-\varepsilon$ model selected as the base turbulence model. For the airfoil simulation, f_ε was set to 1, while f_k was dynamically defined. The value of f_k was instantaneously determined in space based on local mesh conditions and turbulence length scales. The equation for f_k is as follows [12]:

$$f_k = \min(1, 3(\Delta/l)^{2/3}) \tag{10}$$

Where l represents the local turbulence length scale, and Δ denotes the local grid scale. The value of f_k can be dynamically adjusted based on the local mesh and turbulence scale. When the turbulence scale is relatively small, $f_k \approx 1$, and the computation follows the RANS method. When the turbulence scale is larger, $f_k \approx 0$, and the computation approaches the LES method, directly resolving high-turbulence regions.

3.2 Boundary and Solution Settings

In the Fluent simulation, the NACA2415 airfoil fluid domain mesh was imported, and the UDF was compiled and loaded into Fluent, applied to the turbulence equation with the PANS model for computation. To compare the simulation results, additional numerical calculations were conducted using the $k-\varepsilon$ model. The fluid medium was set as air, with viscosity defined by the Sutherland model, allowing it to vary with temperature. The boundary condition was specified as 'pressure-far-field', with a Mach number of 0.4066 (subsonic flow) [13]. For different angles of attack (0 °, 2 °, 4 °, 6 °, 8 °, 10 °, 12 °, 14 °, 15 °, 18 °, 20 °), the x- and y-direction velocity components were assigned accordingly. For instance, at an angle of attack of 10 °, the velocity components were set to 0.984807 (cos 10 °) in the x-direction and 0.173648 (sin 10 °) in the y-direction. The finite volume method (FVM) was used for numerical discretization, with SIMPLEC for pressure-velocity coupling and a second-order discretization scheme. The turbulence model convective term employed the High-Resolution scheme, while the diffusive term adopted the Central Difference scheme, and Second-Order Implicit was applied for temporal discretization. For convergence control, a minimum of 5000 iterations was set, with a residual convergence criterion of 10^5. During the simulation, the lift coefficient was monitored.

4. Computational Results and Validation

4.1 Analysis of Computational Results

The computational results obtained using the PANS model were exported and analyzed in CFD-POST to examine the velocity and pressure distribution around the airfoil. Additionally, the monitored lift coefficient values were compared with the wind tunnel experimental data published by NACA.

(1) Velocity and Streamlines

The computational results for the NACA2415 airfoil were analyzed at a Mach number of 0.4066, a Reynolds number of 10^5, and angles of attack (AoA) of 6 °, 12 °, 15 °, and 20 °. Figures 4 and 5 illustrate the velocity vector fields and streamline diagrams at different angles of attack. As observed in Figure 4, at a low angle of attack (6 °), the velocity distribution remains relatively smooth. The airflow passes over the airfoil surface smoothly, with minimal pressure variation. The velocity above the airfoil is higher than that below it, generating moderate lift. As the airfoil approaches the critical angle of attack (12 °and 15 °), velocity variations become more pronounced around the leading edge and midsection of the airfoil. The upper surface experiences a noticeable increase in velocity, but the flow becomes less uniform, particularly near the trailing edge, where incipient flow separation starts to appear. At a high angle of attack (20 °), the velocity distribution becomes highly irregular, and strong flow separation occurs on the airfoil surface. Particularly on the upper surface, the velocity decreases, and vortex structures form, leading to severe flow separation. This phenomenon significantly reduces lift while increasing drag, negatively impacting aerodynamic performance.

As shown in the streamline diagram (Figure 5), at a low angle of attack (6 °), the airflow remains attached to the airfoil surface with almost no separation. The streamlines are smooth and nearly parallel, following the airfoil contour. The velocity of the streamlines over the upper surface is higher, while that over the lower surface is lower, creating a velocity gradient and pressure difference, which generates lift. At angles of attack near the critical point (12 °and 15 °), localized flow separation begins to appear on the airfoil surface, particularly in the mid-to-rear section of the upper surface. The streamlines start to show noticeable curvature, and irregular vortex structures begin forming near the trailing edge. These vortices are generated because the airflow fails to remain fully attached to the airfoil surface, causing a change in flow direction. At a high angle of attack (20 °), the streamlines in the wake region become highly distorted, and the flow separation region expands significantly. Vortex structures become stronger and more pronounced, leading to high streamline density and chaotic flow patterns. The intensified flow separation results in vortex shedding that concentrates near the trailing edge of the upper surface and may even extend to the lower surface. This vortex formation significantly degrades the aerodynamic performance of the airfoil, leading to lift loss and increased drag.

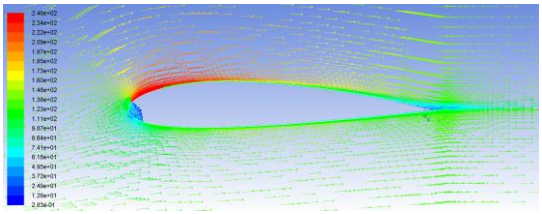

(a) Angle of Attack: 6 °

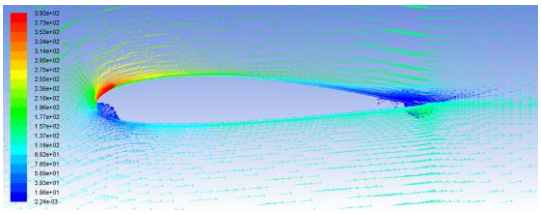

(b) Angle of Attack: 12 °

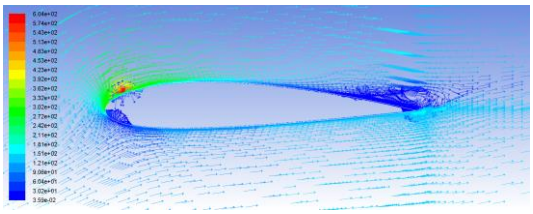

(c) Angle of Attack: 15 °

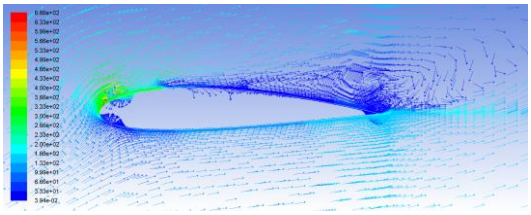

(d) Angle of Attack: 20 °

Figure 4: Velocity Vector Diagrams of the NACA2415 Airfoil at Different Angles of Attack

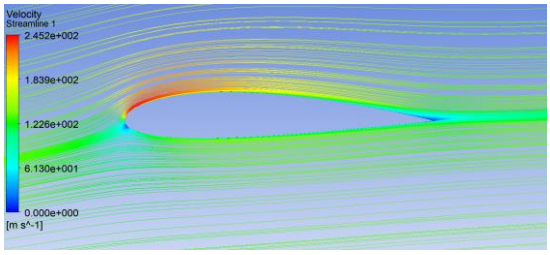

(a) Angle of Attack: 6 °

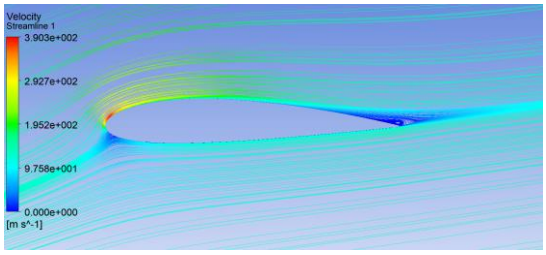

(b) Angle of Attack: 12 °

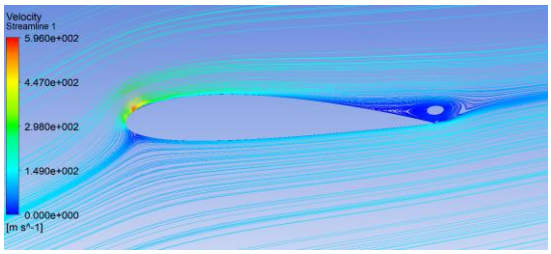

(c) Angle of Attack: 15 °

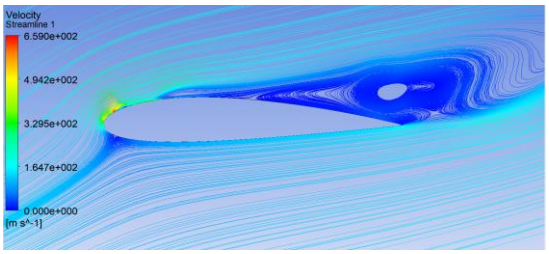

(d) Angle of Attack: 20 °

Figure 5: Streamline Diagrams of the NACA2415 Airfoil at Different Angles of Attack

(2) Pressure Contour Diagram

Figure 6 illustrates the pressure distribution of the NACA2415 airfoil at an angle of attack of 12 °. As shown in the figure, after the airflow contacts the leading edge, it rapidly accelerates, causing a sharp pressure drop and a steep pressure gradient, with the lowest pressure occurring near the leading edge of the upper surface. From the leading edge to the midsection of the upper surface, the pressure gradually increases but remains relatively low, corresponding to a gradual decrease in airflow velocity. In the trailing edge region, the pressure further recovers, and the reduced airflow velocity creates a low-speed region. On the lower surface, the airflow velocity is lower, and the pressure is higher than on the upper surface. The pressure distribution is relatively smooth, and the pressure difference between the upper and lower surfaces is the primary source of lift. By comparing the velocity vector diagram, streamline diagram, and pressure contour diagram, it is evident that the numerical simulation successfully captures the flow field characteristics and lift characteristics of the airfoil. When the angle of attack is below the critical angle, the upper surface experiences higher airflow velocity and lower pressure, forming a negative pressure region that contributes to lift generation. Meanwhile, the lower surface maintains a lower velocity and higher pressure, which helps support the airfoil and sustain lift.

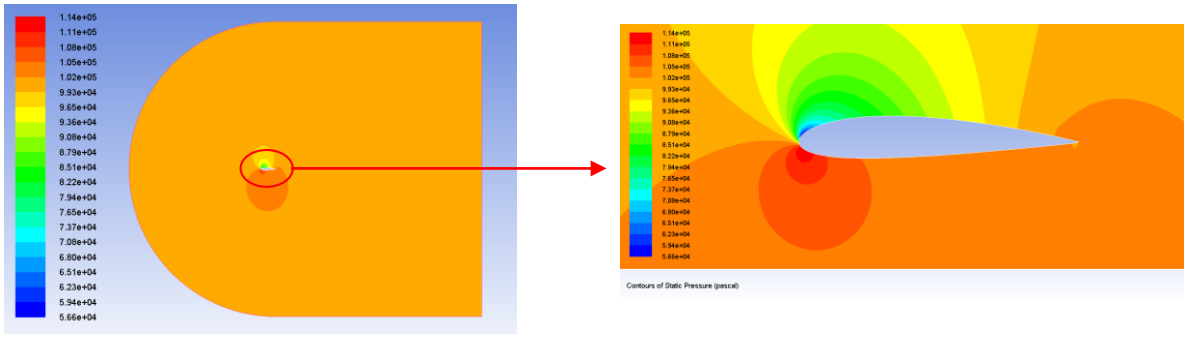

Figure 6: Pressure Contour Diagram of the NACA2415 Airfoil at an Angle of Attack of 12 °

4.2 Comparison with Experimental Data

The lift coefficient (C_L) is a critical parameter that directly affects the aerodynamic performance of the airfoil. NACA has published experimental wind tunnel data for lift coefficients, providing a reference for validation. Figure 7 shows the monitored lift coefficient during the numerical simulation. Taking an angle of attack of 10 °as an example, after 5000 iterations, the lift coefficient stabilizes at approximately 1.173, which is in close agreement with the wind tunnel test data of 1.22.

Figure 8 presents a comparison between the numerically computed lift coefficients and the experimental data for the NACA2415 airfoil at different angles of attack. The results indicate that the numerical simulations exhibit the same trend as the experimental values. The errors between the PANS model and the k-ε model vary slightly: At low angles of attack, where the airflow over the airfoil surface remains relatively stable, both models exhibit small deviations from the experimental results. As the angle of attack increases, severe flow separation occurs, and the PANS model demonstrates higher simulation accuracy, with smaller deviations in lift coefficient compared to experimental values. These results confirm that the PANS model used in this study is highly reliable for simulating the external aerodynamic characteristics of airfoils, especially under conditions of high turbulence intensity and complex flow separation.

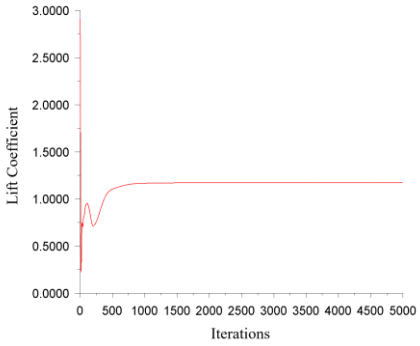

Figure 7: Monitoring of Lift Coefficient in Numerical Simulation

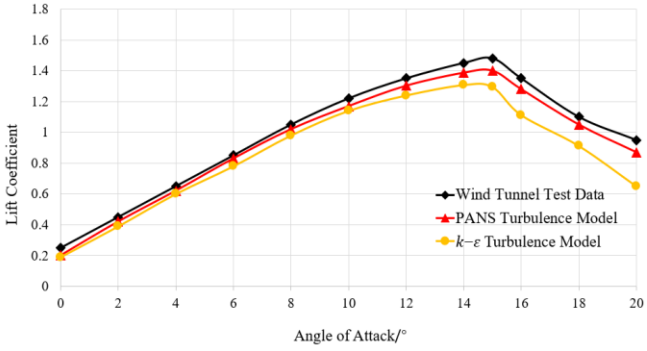

Figure 8: Comparison of Computed and Experimental Lift Coefficients at Different Angles of Attack

5. Conclusions

In this study, the turbulence model was modified using the User-Defined Function (UDF) feature to construct a Partially-Averaged Navier-Stokes (PANS) model. Numerical simulations were conducted on the NACA2415 airfoil, and the results were compared with wind tunnel experimental

data. The conclusions are as follows:

(a) Based on the *k*-*ε* model, the UDF function was utilized to modify the turbulence model, forming the PANS model. The f_k value (the ratio of unresolved turbulent kinetic energy to total turbulent kinetic energy) was dynamically defined, allowing it to be instantaneously adjusted based on local mesh conditions and turbulence length scale. This implementation enabled a smooth transition from the RANS model to the LES model, effectively balancing computational cost and simulation reliability.

(b) A 3D model of the NACA2415 airfoil was created, and a structured mesh was generated. The mesh adaptation function in Fluent was used to ensure the reasonability of the wall '*Y*+' values. The 'pressure-far-field' was set as the computational boundary condition, and numerical simulations were conducted using the PANS model. The velocity distribution, streamlines, and pressure characteristics of the airfoil surface were analyzed at different angles of attack.

(c) By comparing the computed lift coefficients with wind tunnel experimental data, the high reliability of the turbulence model used in this study for external airfoil characteristic simulations was demonstrated. Analysis of the airfoil's aerodynamic behavior revealed that as the angle of attack increases, the velocity and pressure difference between the upper and lower surfaces grow, leading to an increase in the lift coefficient until it reaches the critical angle of attack. Beyond this point, the flow becomes more turbulent, vortex formation intensifies, and the lift coefficient decreases, which is consistent with the aerodynamic performance observed in the NACA2415 wind tunnel experiments.

Acknowledgements

This research is supported by the NanHang JinCheng College 2023 School-Level Scientific Research Fund Project "Study on Wake Vortex Dissipation Characteristics under Multiple Environmental Variables during Aircraft Approach" (Project No.: XJ202310).

References

[1] Girimaji, S. S. Partially-averaged Navier–Stokes model for turbulence: a Reynolds-averaged Navier–Stokes to direct numerical simulation bridging method [J]. Journal of Applied Mechanics, 2006, 73(3), 413-421.

[2] Basara, B., Girimaji, S. S., & Jakirlić, S. PANS methodology applied to elliptic-relaxation based eddy-viscosity turbulence model [J]. International Journal of Heat and Fluid Flow, 2011,32(3), 508-519.

[3] Huang Biao, Wang Guoyu, Quan Xiaobo, Chen Guanghao. Application of PANS Model in Cavitating Turbulent Flow Numerical Calculation. Journal of Applied Mechanics, 2011, 28(4): 339-344.

[4] Du Ruofan, Yan Chao, Luo Dahai. Performance Analysis of PANS Method in Numerical Simulation of Flow Around Twin Cylinders. Journal of Beijing University of Aeronautics and Astronautics, 2015, 41(8): 1503-1509.

[5] Wang Peng, Li Ming, Wang Wei. Comparison of SAS and PANS Models in Flow around a Cylinder. Journal of Aerodynamics, 2019, 37(4): 530-538.

[6] Abbott, I. H., & von Doenhoff, A. E. Summary of Airfoil Data[M]. NACA Report No. 824.1959.

[7] G. K. Batchelor, An Introduction to Fluid Dynamics[M]. Cambridge, UK: Cambridge University Press, 2000

[8] Yu Yunyun, Zhou Daqing, Yu An, et al. Numerical Simulation of Cavitation Characteristics in an Axial Flow Pump Based on the Modified PANS Model[J]. Journal of Drainage and Irrigation Machinery Engineering, 2022, 40(12): 1204-1211.

[9] Huang R, Luo X, Ji B, et al. Turbulent flows over a backward facing step simulated using a modified Partially-Averaged Navier-Stokes model [J]. Journal of Fluids Engineering, 2017, 139(4):044501.

[10] Launder B.E, Spalding D.B, Lectures in Mathematical Models of Turbulence[M]. Academic Press, London, 1972.

[11] Davidson L. The PANS k-epsilon model in a zonal hybrid RANS-LES formulation[J]. International Journal of Heat & Fluid Flow, 2014, 46(4):112-126.

[12] Chen, S., & Zhang, X. A modified PANS approach for the simulation of unsteady flow and cavitation in turbomachinery [J]. Journal of Fluid Engineering, 2020, 142(3), 031301.

[13] Doe, J., & Smith, A. Experimental Study of Subsonic Flow Past a Body of Revolution[J]. Journal of Fluid Mechanics, 2020, 250(3), 453-467.